Steady state operation simulation of the Francis-99 turbine by means of advanced turbulence models

[1,2,3]Gavrilov A., [1,2,3]Dekterev A., [1,2,3]Minakov A., [1,2,3] Platonov D., [1,2,3]Sentyabov A.

[1]Siberian Federal University, Krasnoyarsk, Svobodniy 79, 660079 Russia
[2]Institute of Thermophysics SB RAS, Novosibirsk, Lavrentyeva 1, 630090 Russia
[3]Novosibirsk State University, Novosibirsk, Pirogova 2, 630090 Russia

E-mail: gavand@yandex.ru, dekterev@mail.ru, tov-andrey@yandex.ru, platonov-08@yandex.ru, , sentyabov_a_v@mail.ru

Abstract.

1. Introduction

Hydropower resources are the major renewable source of the electric power. At the present time, hydraulic power plants are being built and modernized. Accordingly, many scientific and engineering problems arise in the field of flow dynamics, such as finding of the power and efficiency of the turbine, calculation of the cavitation, pressure pulsations and forces on the turbine equipment.

Numerical simulation of flow in turbines is a useful tool for design of hydraulic turbines. At the same time, this is a very complicated problem due to complex shape of the flow path, turbulence, rotated runner, swirled flow under the runner and large-scale unsteady coherent structures. These features impose strict requirements on the turbulence models. Two-equation turbulence models (k-ε and k-ω) are most widely used in industrial applications. Large eddy simulation (LES) and hybrid RANS/LES methods are increasingly used for unsteady large-scale phenomena in complicated flows. At last, differential Reynolds stress model can accurately reproduce phenomena related to anisotropy of the turbulent fluctuations. In-house CFD code SigmaFlow is used for simulations the flow in Francis-99 turbine by different models in steady-state operation modes.

2. Mathematical model and numerical method

The simulations were based on the geometry and parameters of the operating points provided by organizers of the Francis-99 workshop II [1]. Computational domain consists of wicket gate, runner and draft tube (Fig. 1). Computational meshes includes about 4.3 mln. polyhedral cells. The simulations were performed by means of in-house CFD code SigmaFlow [2, 3]. Rotated reference frame in absolute velocity formulation was used for modeling of the runner rotation.

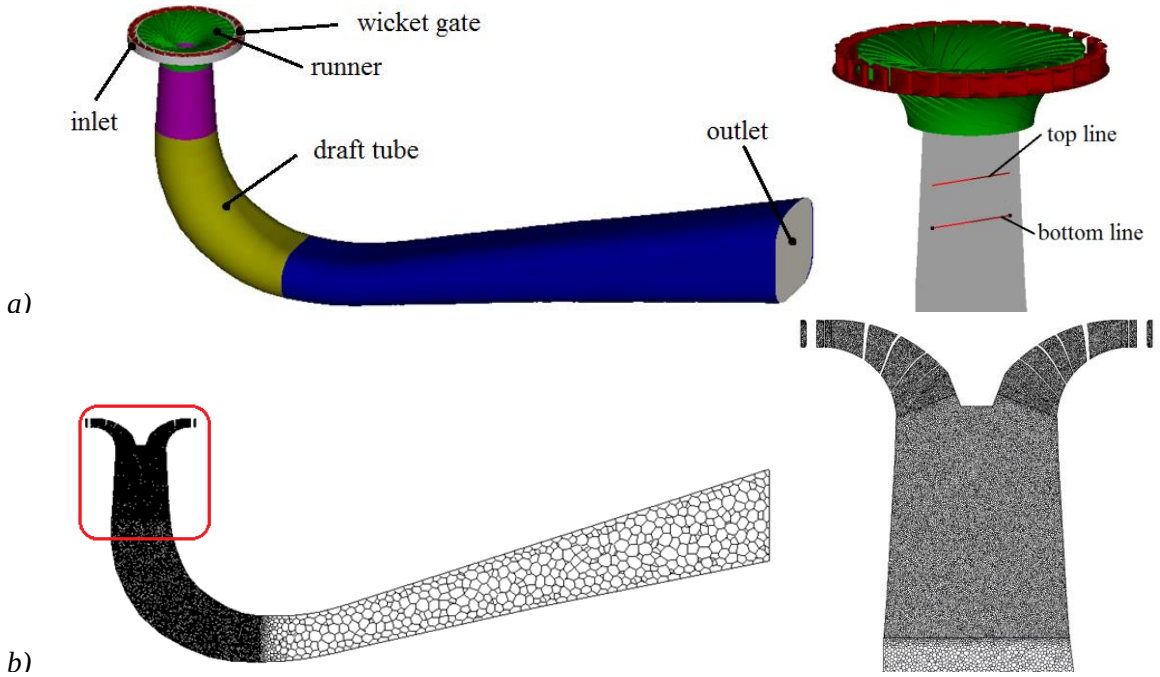

Figure 1. Francis-99 test case; *a*) computational domain; *b*) mesh in central cross-section

Below, the basic equations of the mathematical models expressing the conservation laws in the rotating reference frame are presented. Einstein summation convention is used.
The continuity equation (conservation of mass):

$$\frac{\partial u_i}{\partial x_i} = 0$$

Momentum equations (conservation of momentum) in a rotating reference frame for absolute velocities:

$$\frac{\partial \rho u_i}{\partial t} + \frac{\partial}{\partial x_j}\left(\rho u_j^r u_i\right) = -\frac{\partial p}{\partial x_i} + \frac{\partial}{\partial x_j}(\tau_{ij}^{\mathrm{m}} + \tau_{ij}^{\mathrm{t}}) - \rho \varepsilon_{ijk} \Omega_j u_k$$

Where: u_i – absolute velocity components, u_j^r – relative velocity components, τ_{ij}^{m} – viscous stress tensor, τ_{ij}^{t} – turbulent stress tensor, Ω – angular velocity of runner rotation, p – static pressure, ρ – density, ε_{ijk} – Levi-Civita symbol.

Components of the viscous stress tensor are defined as:

$$\tau_{ij}^{\mathrm{m}} = \mu\left(\frac{\partial u_i}{\partial x_j} + \frac{\partial u_j}{\partial x_i}\right)$$

where μ is dynamic molecular viscosity.

Several turbulence modeling approach were used. There were eddy viscosity models (k-ω SST, [4, 5], ζ-f [6]) and differential Reynolds stress model [7]. Reynolds stress $\rho\overline{u_i'u_j'}$ transport equations are solved in RSM model:

$$\frac{\partial}{\partial t}\left(\rho\overline{u_i'u_j'}\right)+\frac{\partial}{\partial x_l}\left(\rho u_l\overline{u_i'u_j'}\right)=\rho\left(P_{ij}+Diff_{ij}-\varepsilon_{ij}+\phi_{ij}\right).$$

Where P_{ij} is production term, $Diff_{ij}$ is diffusion term, ε_{ij} is dissipation term, ϕ_{ij} is pressure strain term. Production term does not require any modeling:

$$P_{ij}=-\left(\overline{u_i'u_l'}\frac{\partial u_j}{\partial x_l}+\overline{u_j'u_l'}\frac{\partial u_i}{\partial x_l}\right).$$

Diffusion term is modeled by means of turbulent viscosity:

$$Diff_{ij}=\frac{\partial}{\partial x_l}\left(\left(\mu+\frac{\mu_t}{\sigma_k}\right)\frac{\partial\overline{u_i'u_j'}}{\partial x_l}\right),\ \sigma_k=0.82,$$

where turbulent viscosity:

$$\mu_t=\rho C_\mu\frac{k^2}{\varepsilon},\ k=\frac{1}{2}\overline{u_i'u_i'},\ C_\mu=0.09.$$

Dissipation tensor ε_{ij} is modeled by isotropic tensor:

$$\varepsilon_{ij}=\frac{2}{3}\delta_{ij}\varepsilon,$$

Where scalar dissipation rate ε is computed with a transport equation:

$$\frac{\partial\rho\varepsilon}{\partial t}+\frac{\partial}{\partial x_j}\left(\rho u_j\varepsilon\right)=\frac{\partial}{\partial x_j}\left(\left(\mu+\frac{\mu_t}{\sigma_k}\right)\frac{\partial\varepsilon}{\partial x_j}\right)+\rho\frac{C_{\varepsilon1}P_k-C_{\varepsilon2}\varepsilon}{T},$$

$$T=\frac{k}{\varepsilon},\ \sigma_\varepsilon=1.0,\ C_{\varepsilon1}=1.44,\ C_{\varepsilon2}=1.92$$

Pressure strain term is modeled by SSG strain model [7].

In constructing two-equation models of turbulence for defining the components of Reynolds' stress tensor τ_{ij}^{t}, Boussinesq's hypothesis of isotropic turbulent viscosity is used:

$$\tau_{ij}^{t} = \mu_{t}\left[\left(\frac{\partial u_i}{\partial x_j}+\frac{\partial u_j}{\partial x_i}\right)-\frac{2}{3}\delta_{ij}\rho k\right]$$

The discharge, obtained from the experimental data, was fixed at the inlet and outlet boundaries. Speed of the runner rotation was -34.83 rad/s according to experimental parameters. The density of the water was $\rho = 999.8$ kg/m^3 and the molecular viscosity was $\mu = 9.568 \cdot 10^{-4}$ Pa·s.

Discretization of transport equations was carried out by the control volume method on unstructured grids. Coupling of the velocity and pressure fields for incompressible flow was realized using the SIMPLE-like procedure. For the approximation of the convective terms in the equations for momentum components up-wind scheme was used. For the approximation of the convective terms in the equations for turbulent characteristics up-wind scheme was used. Unsteady calculation were performed to obtain steady or averaged solution. Earlier some calculations have shown that this technique can reliably consider averaged velocity and large-scale turbulent fluctuations in water turbines [8–9].

3. Results of Francis-99 simulations

In case of fixed discharge, the calculated torque on the runner is overestimated noticeably in the considered operating points (Table 1). Models *k*-ω SST and ζ-*f* calculates the same value of the torque, but RSM model obtains the lesser one. The discrepancies of the torque vary from 8 to 15%.

Table 1. Torque on the runner, N·m

	PL	BEP	HL
k-ω SST	487	703	835
ζ-*f*	486	702	833
RSM	465	680	810
experiment	421	621	744

At the best efficiency operating point, the flow under the runner is steady and weakly swirled (Fig 2*b*, 3*b*). There is small recirculation region under the runner hub. This zone generates long wake along the turbine axis. There is a straight weak vortex at the turbine axis. The axial velocity profiles have the maximum around the wake (Fig 2*b*, 4*b*). The calculated axial velocity profiles closely agree with the experimental profiles. There is no graphical differences between results of the eddy viscosity models (*k*-ω SST and ζ-*f*).

At the part load operating point, large-scale unsteady vortex rope forms under the runner (Fig 2*a*, 3*a*). There are many small vortices under the runner blades near the draft tube wall (Fig 3*a*). Calculated axial velocity profiles show a recirculation zone near the axis, but experimental profiles do not show it (Fig. 4*a*). Therefore, the calculated vertical velocity is significantly above the experimental one at the axis in case of all the models.

At the high load operating point, there is a weak vortex under the runner hub (Fig 2*c*, 3*c*). The vortex undergoes instability and has a spiral form at a distant of the runner. Calculated axial velocity

profiles agree with experimental data but they show significant numerical viscosity for all the models (Fig. 4*c*).

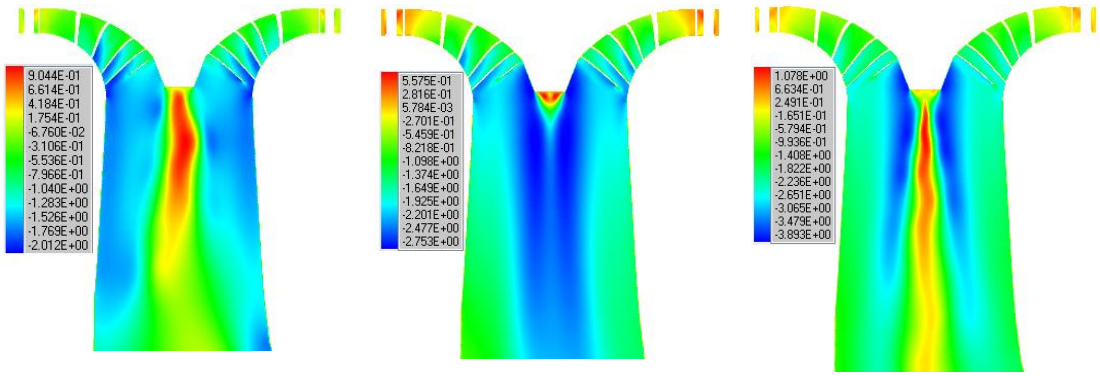

a *b* *c*

Figure 2. Instant vertical velocity in the central plane (ζ-*f* model): *a*) part load, *b*) best efficiency point, *c*) high load.

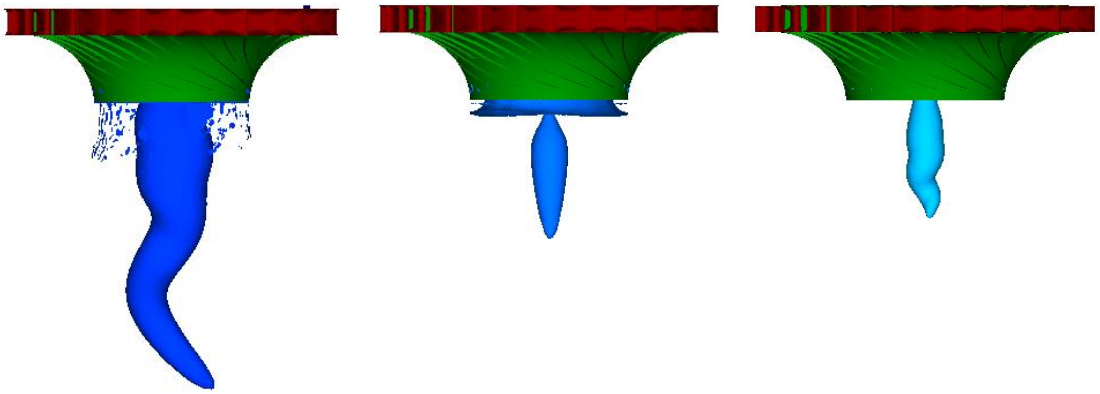

a *b* *c*

Figure 3. Vortices in the draft tube, visualized by iso-pressure surface (ζ-*f* model): *a*) part load, *b*) best efficiency point, *c*) high load.

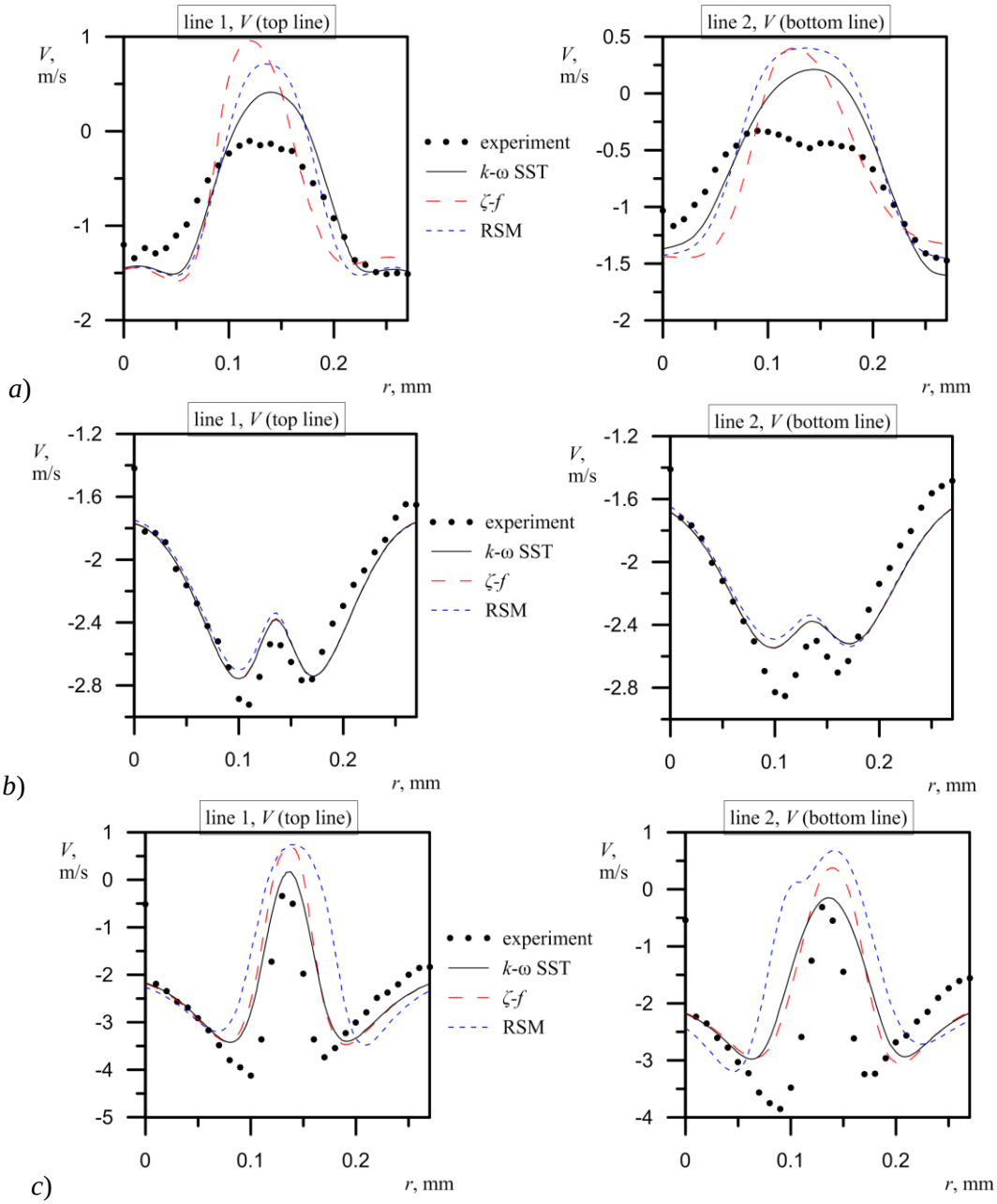

Figure48. Averaged axial velocity component in the draft tube: *a*) part load; *b*) best efficiency point, *c*) high load.

4. Conclusions

Thus, the calculations show flow patterns depending on the operating point of the turbine. At the best efficiency point the flow in the draft tube is steady and there is a weak straight vortex along the turbine axis under the runner. At part load operating point there is a wide strong vortex rope that rotates near the draft tube wall. At high load operating point there is a weak vortex under the runner hub which form becomes spiral at a distant of the runner.

The calculated data agree with experimental results well for best efficiency point. For high load operating points there is only qualitative agreement between calculation and experimental results. For

part load operating points there is significant discrepancy between calculated and experimental results. For all the regimes there is no noticeable difference between the results of the eddy viscosity models *k*-ω SST and ζ-*f*.

Acknowledgements
This work was supported by Russian Science Foundation (project No. 16-19-00138).

References

[1] https://www.ntnu.edu/nvks/test-case.
[2] Gavrilov A.A., Dekterev A.A. and Sentyabov A.V., Modeling of Swirling Flows with Coherent Structures Using the Unsteady Reynolds Stress Transport Model // Fluid Dynamics, 2015, Vol. 50, No 4, pp. 471 – 482.
[3] Gavrilov A.A., Sentyabov A.V., Dekterev A.A., Hanjalic K. Vortical structures and pressure pulsations in draft tube of a Francis-99 turbine at part load: RANS and hybrid RANS/LES analysis // International Journal of Heat and Fluid Flow, 2016, June (online available), DOI: 10.1016/j.ijheatfluidflow.2016.05.007 –
[4] Menter F.R. 1994 Two Equation Eddy Viscosity Turbulence Models for Engineering Applications *AIAA J.* **32**, № 8, 1598-1605
[5] Menter F.R., Kuntz M. and Langtry R. 2003 Ten Years of Experience with the SST Turbulence Model Turbulence, Heat and Mass Transfer 4 (Begell House Inc.) In K. Hanjalic, Y. Nagano, and M. Tummers, editors 625–32
[6] Hanjalić K., Popovac M. and Hadžiabdić M. A robust near-wall elliptic relaxation eddy viscosity turbulence model for CFD. Int. J. Heat Fluid Flow, 25(6):1047-1051, 2004.
[7] Speziale C.G., Sarkar S. and Gatski T.B. Modeling the pressure–strain correlation of turbulence: an invariant dynamical system approach. J. Fluid Mech., 227:245-272, 1991.
[8] Minakov A.V., Platonov D.V., Dekterev A.A., Sentyabov A.V., Zakharov A.V. The numerical simulation of low frequency pressure pulsations in the high-head Francis turbine // Computers and Fluids, 2015, Vol. 111, pp. 197-205, DOI:10.1016/j.compfluid.2015.01.007
[9] Minakov A.V., Platonov D.V., Dekterev A.A., Sentyabov A.V., Zakharov A.V. The analysis of unsteady flow structure and low frequency pressure pulsations in the high-head Francis turbines // International Journal of Heat and Fluid Flow, 2015, Vol. 53, pp. 183-194, DOI: 10.1016/j.ijheatfluidflow.2015.04.001